© 2024. Published by The Company of Biologists Ltd | Development (2024) 151, dev202098. doi:10.1242/dev.202098

Notch signalling influences cell fate decisions and HOX gene induction in axial progenitors

Fay Cooper[1,2,*], Celine Souilhol[1,2,3], Scott Haston[4,5], Shona Gray[5], Katy Boswell[1,2], Antigoni Gogolou[1,2], Thomas J. R. Frith[1,2], Dylan Stavish[1,2], Bethany M. James[1,2], Daniel Bose[1,2], Jacqueline Kim Dale[5] and Anestis Tsakiridis[1,2,*]

ABSTRACT

The generation of the post-cranial embryonic body relies on the coordinated production of spinal cord neurectoderm and presomitic mesoderm cells from neuromesodermal progenitors (NMPs). This process is orchestrated by pro-neural and pro-mesodermal transcription factors that are co-expressed in NMPs together with Hox genes, which are essential for axial allocation of NMP derivatives. NMPs reside in a posterior growth region, which is marked by the expression of Wnt, FGF and Notch signalling components. Although the importance of Wnt and FGF in influencing the induction and differentiation of NMPs is well established, the precise role of Notch remains unclear. Here, we show that the Wnt/FGF-driven induction of NMPs from human embryonic stem cells (hESCs) relies on Notch signalling. Using hESC-derived NMPs and chick embryo grafting, we demonstrate that Notch directs a pro-mesodermal character at the expense of neural fate. We show that Notch also contributes to activation of HOX gene expression in human NMPs, partly in a non-cell-autonomous manner. Finally, we provide evidence that Notch exerts its effects via the establishment of a negative-feedback loop with FGF signalling.

KEY WORDS: Axial progenitors, HOX, Neuromesodermal progenitors, NMPs, Notch signalling, Human, Chick

INTRODUCTION

The formation of the amniote embryonic body takes place in a head-to-tail (anterior-posterior) direction and it is driven by developmentally plastic axial progenitors, which can generate both spinal cord neurectoderm and presomitic/paraxial mesoderm, the precursor of the vertebral column/trunk musculature [thus termed neuromesodermal progenitors (NMPs); reviewed by Wymeersch et al., 2021)]. NMPs arise around the end of gastrulation/early somitogenesis, within a posterior growth region that encompasses the node–anterior primitive streak border (NSB) and the caudal lateral epiblast (Brown and Storey, 2000; Cambray and Wilson, 2002, 2007; Guillot et al., 2021; Mugele et al., 2018; Wymeersch et al., 2016). They are marked by the co-expression of pro-neural and pro-mesodermal transcription factors, such as *Sox2*, *T* (brachyury; *TBXT* in humans), *Tbx6* and *Cdx2* (Gouti et al., 2017; Guillot et al., 2021; Javali et al., 2017; Koch et al., 2017; Martin and Kimelman, 2012; Olivera-Martinez et al., 2012; Tsakiridis et al., 2014; Wymeersch et al., 2016). The antagonistic interaction between these lineage-specific transcription factors determines the balanced production of neural versus mesodermal cell types from NMPs (Gouti et al., 2017; Koch et al., 2017). NMPs are also marked by the expression of Hox gene family members [arranged as paralogous groups (PGs) in four distinct chromosomal clusters: A, B, C, and D], which are activated within the posterior growth region in a sequential manner reflecting their 3′-to-5′ genomic order (Gouti et al., 2017; Guillot et al., 2021; Neijts et al., 2017; Wymeersch et al., 2019). The latter process is tightly linked to the assignment of a positional identity in the nascent axial progenitor derivatives before their allocation along the developing embryonic anteroposterior axis (reviewed by Deschamps and Duboule, 2017).

The NMP niche relies on the activity of key posteriorising signalling pathways, such as Wnt and FGF. These trigger the transcription factor networks operating within NMPs, which, in turn, potentiate, via positive feedback, Wnt/FGF activity within the posterior growth region during axis elongation (Amin et al., 2016; Blassberg et al., 2022; Martin and Kimelman, 2012; Mukherjee et al., 2022; Young et al., 2009). The balance between these two signalling pathways appears to orchestrate NMP cell fate decisions as Wnt/FGF have been shown to be linked to both progenitor maintenance and differentiation toward early neural and presomitic mesoderm cells (Amin et al., 2016; Anand et al., 2023; Cooper et al., 2022; Delfino-Machín et al., 2005; Diez del Corral et al., 2002; Gouti et al., 2017; Martin and Kimelman, 2012; Semprich et al., 2022; Wind et al., 2021; Young et al., 2009). In line with these findings, Wnt and FGF signalling agonists are the two main components of protocols for the generation of NMP-like cells and their earliest mesodermal and neural derivatives from mouse and human pluripotent stem cells *in vitro* (Chal et al., 2015; Cooper et al., 2022; Frith et al., 2018; Lippmann et al., 2015; Turner et al., 2014; Verrier et al., 2018; Wind et al., 2021). Moreover, Hox gene expression in the posterior growth region/NMPs is also driven largely by Wnt and FGF activity via crosstalk with the two key posteriorising transcription factors *CDX2* and *TBXT* (Amin et al., 2016; Chawengsaksophak et al., 2004; Gogolou et al., 2022; Metzis et al., 2018; Neijts et al., 2017, 2016).

The other key developmental signalling pathway that has been found to be active in the posterior growth region/NMP niches is

[1]School of Biosciences, The University of Sheffield, Sheffield S10 2TN, UK. [2]Neuroscience Institute, The University of Sheffield, Sheffield S10 2TN, UK. [3]Biomolecular Sciences Research Centre, Department of Biosciences and Chemistry, Sheffield Hallam University, Sheffield S1 1WB, UK. [4]Developmental Biology and Cancer, Birth Defects Research Centre, UCL GOS Institute of Child Health, London WC1N 1EH, UK. [5]Division of Cell and Developmental Biology, School of Life Sciences, University of Dundee, Dundee DD1 4HN, UK.

*Authors for correspondence (f.cooper@sheffield.ac.uk; a.tsakiridis@sheffield.ac.uk)

F.C., 0000-0002-5340-619X; S.H., 0000-0003-3928-4808; D.S., 0000-0002-1441-2028; D.B., 0000-0002-0276-6486; A.T., 0000-0002-2184-2990

Handling Editor: James Wells
Received 16 June 2023; Accepted 20 December 2023

Development (2024) 151, dev202098. doi:10.1242/dev.202098

Notch. Notch signalling is activated through the interaction of receptors and ligands expressed by neighbouring cells. In mammals, there are four transmembrane receptors (NOTCH1-4), which bind to five Notch transmembrane ligands (DLL1, DLL3, DLL4, JAG1 and JAG2). Once bound, the Notch receptor undergoes two successive proteolytic cleavage events mediated by ADAM10 and γ-secretase, which releases the intracellular Notch domain (NICD) into the cell nucleus, allowing it to bind to the Notch signalling transcription factor RBPJκ (also known as CSL) (Carrieri and Dale, 2016; Shen et al., 2021). Several Notch signalling components are expressed in NMPs and their immediate neural and mesodermal derivatives, from late gastrulation and throughout embryonic axis elongation (Akai et al., 2005; Bettenhausen et al., 1995; Dunwoodie et al., 1997; Williams et al., 1995; Wymeersch et al., 2019; Zhang and Gridley, 1998). Moreover, the attenuation or overexpression of many of these components leads to severe posterior patterning defects (Akai et al., 2005; Dale et al., 2003; de la Pompa et al., 1997; Donoviel et al., 1999; Nowotschin et al., 2012; Oka et al., 1995; Souilhol et al., 2015). Notch signalling has also been found to crosstalk with the principal posteriorising Wnt and FGF signalling pathways during axis elongation (Akai et al., 2005; Galceran et al., 2004; Gibb et al., 2009; Nakaya et al., 2005), and the expression of Notch signalling components in the posterior growth region is driven by key NMP regulators – Wnt/FGF targets such as *T/TBXT* and *Cdx2* (Amin et al., 2016; Gogolou et al., 2022; Guibentif et al., 2021; Koch et al., 2017). Collectively, these data suggest that Notch signalling may be a crucial component of the NMP niche and interlinked with the well-established signalling pathways regulating NMP specification and maintenance. However, it is still unclear exactly how Notch influences NMP ontogeny.

Here, we investigated the role of Notch signalling in axial progenitors using the differentiation of human embryonic stem cells (hESCs) toward NMPs as a model. We show that Notch attenuation during NMP induction impairs the activation of pro-mesodermal transcription factors and global HOX gene activation whilst promoting an early neural character. Our results indicate that Notch-driven pro-mesodermal/HOX gene expression control is mediated via the establishment of a feedback loop with FGF signalling. We provide evidence that the induction of certain HOX genes in hESC-derived NMPs may be mediated by Notch in a non-cell-autonomous fashion. Finally, Notch signalling inhibition in chick embryonic NMPs dramatically alters their engraftment behaviour and impairs their capacity to generate paraxial mesoderm cells, biasing them instead toward a ventral neural/floor plate cell fate. Together, these findings suggest that Notch contributes, together with Wnt and FGF, to the primary signalling axis within the posterior growth region that orchestrates NMP cell fate decisions and positional identity acquisition.

RESULTS AND DISCUSSION

Notch signalling mediates the induction of pro-mesodermal and HOX genes in NMPs

To gain an insight into the dynamics of Notch activity within the NMP niche, we first mapped in detail the expression of Notch signalling components in the posterior growth region of both chicken and mouse embryos. *In situ* hybridisation analysis revealed the presence of Notch-associated transcripts, at variable levels, in the NMP-containing caudal lateral epiblast as well as the primitive streak (Fig. S1A), in line with previous reports (Bettenhausen et al., 1995; Dunwoodie et al., 1997; Williams et al., 1995; Wymeersch et al., 2019). Moreover, we have previously shown that the *in vitro* generation of NMPs following treatment of human pluripotent stem cells (hPSCs) with the Wnt agonist CHIR99021 (CHIR) and recombinant FGF2 for 3 days is accompanied by an upregulation of Notch signalling-associated transcripts (Frith et al., 2018; Wind et al., 2021). Interrogation of published single-cell RNA-sequencing data from time-course analysis of differentiating human induced pluripotent stem cells further confirmed the expression of Notch components in *in vitro*-derived NMPs (Diaz-Cuadros et al., 2020) (Fig. S1B).

To define the role of the increase in Notch signalling activity during the transition of pluripotent cells toward a neuromesodermal-potent state, we generated NMPs from WA09 (H9) hESCs in the presence of the Notch/γ-secretase inhibitor DAPT or dimethyl sulfoxide (DMSO; control) (Fig. 1A). Quantitative PCR (qPCR)-based analysis of DAPT-treated NMP cultures (NOTCHi) revealed that they expressed significantly reduced levels of *HES5*, *HES1* and *NOTCH1* compared with controls, indicating effective attenuation of Notch signalling (Fig. S2A). Moreover, NOTCHi NMPs were marked by a considerable reduction in the expression of pro-mesodermal/NMP markers such as *TBXT*, *TBX6* and *CDX1* and a concomitant increase in the transcription of the pro-neural NMP marker *SOX2* (Fig. 1B). Similar changes in TBXT and SOX2 were detected at the protein level (Fig. 1C, Fig. S2B), whereas we found no increase in the expression of pluripotency-associated [OCT4 (POU5F1) and NANOG] or later spinal cord neuroectodermal (PAX6 and SOX1) markers, which remained low/undetected (Fig. S2C-E). Similar results were obtained following further 3-day (D) culture of cells under NMP-inducing conditions in the presence of DAPT (Fig. S2F-I), indicating that the attenuation of *TBXT*/*TBX6* expression we observe in D3 hESC-derived NMPs upon Notch inhibition is not due to a delay in the acquisition of pro-mesodermal character. To examine further the effect of Notch signalling on the mesoderm potential of hESC-derived NMPs, we subjected D3 NOTCHi NMPs to presomitic mesoderm-inducing conditions (high WNT/FGF signalling activity; Frith et al., 2018) for 3 days in the presence and absence of DAPT (Fig. 1D). We found that the resulting D6 NOTCHi NMP-derived cultures failed to upregulate TBXT and TBX6 and retained higher levels of SOX2 expression compared with controls (Fig. 1E,F). Together, these results suggest that NOTCH signalling mediates the pro-mesodermal character of NMPs during their specification from pluripotent cells at the expense of a spinal cord pre-neural $SOX2^{+}$ identity.

We next examined the global activation of HOX genes, a major hallmark of Wnt/FGF-driven acquisition of a posterior axial and NMP identity (Cooper et al., 2022; Gogolou et al., 2022; Gouti et al., 2017; Guillot et al., 2021; Wymeersch et al., 2019), in DAPT-treated cultures. We found that NOTCHi hESC-derived NMPs exhibited a marked reduction in the expression of most HOX PG members examined, particularly those belonging to the *HOXC* and *HOXD* clusters, compared with the DMSO controls (Fig. 1C,G). Moreover, we found that the DAPT-driven perturbation in HOXC9 protein expression (Fig. 1C) occurred in SOX2-positive/TBXT-positive as well as SOX2-positive/TBXT-negative cell populations (Fig. S2J) suggesting that impaired activation of HOX gene clusters occurs irrespectively of the expression status of TBXT, a transcription factor that has been found to control directly HOX gene transcription in human NMPs (Gogolou et al., 2022). Together, these findings indicate that Notch signalling modulates the induction of a posterior axial identity and colinear activation of HOX PG family members by Wnt and FGF, as pluripotent cells transit toward NMPs.

Non-cell-autonomous control of HOX gene expression in human NMPs is partly Notch driven

The striking effect of DAPT on the induction of various HOX genes in hESC-derived NMPs prompted us to examine further the links

Development (2024) 151, dev202098. doi:10.1242/dev.202098

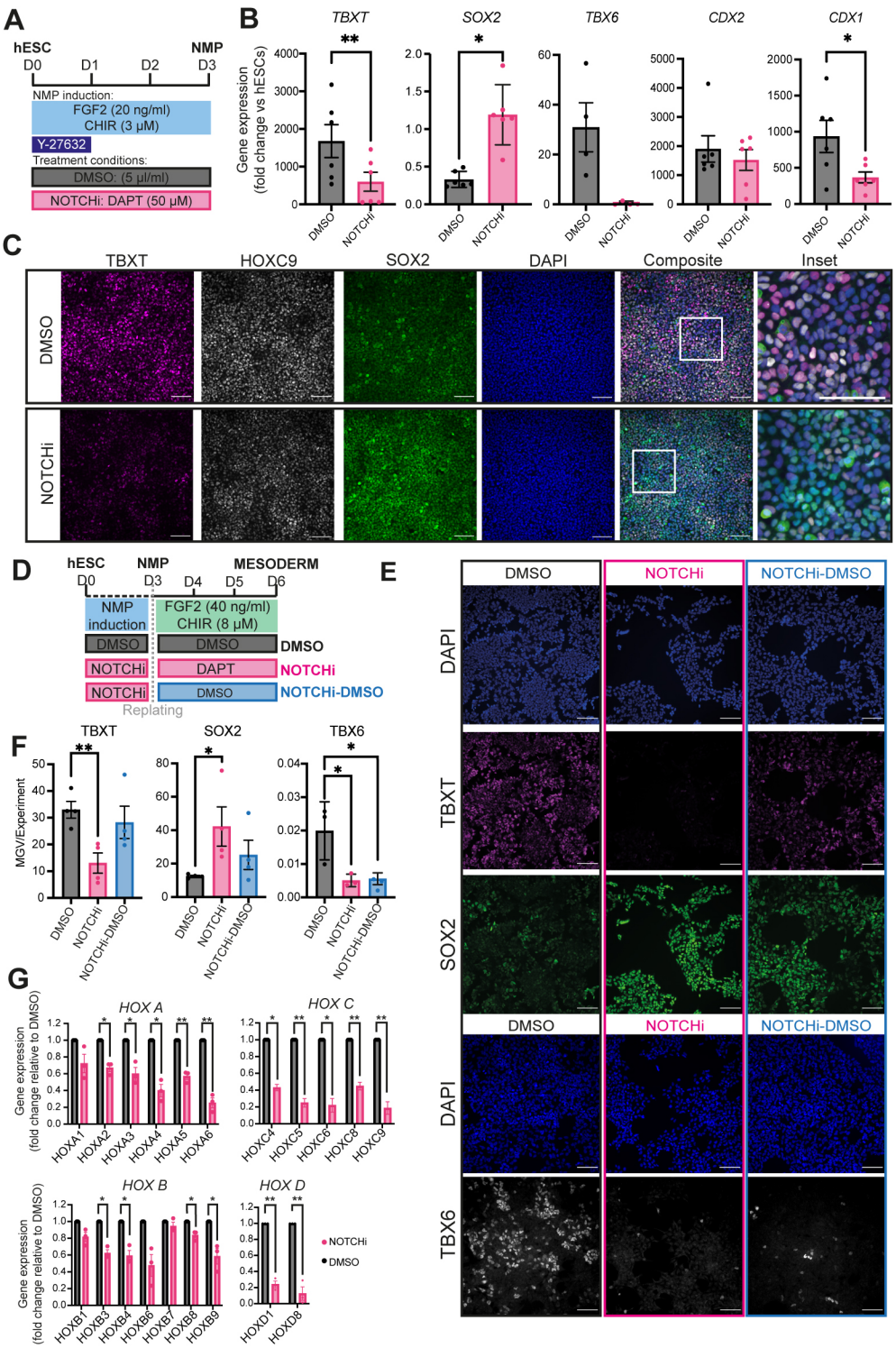

Fig. 1. Notch inhibition impairs the induction of pro-mesodermal/HOX genes during NMP specification *in vitro*. (A) Schematic of the treatment conditions used to generate NOTCHi or DMSO control NMPs from hESCs. (B) qPCR expression analysis of key NMP markers in hESC-derived NOTCHi/control NMPs. Error bars represent mean±s.e.m. (n=4-6 independent experiments). *P≤0.05, **P≤0.01 (paired, two-tailed t-test). (C) Immunofluorescence analysis of the expression of HOXC9, TBXT and SOX2 in NMPs treated with DMSO or DAPT. Boxed areas in composite images are shown at higher magnification to the right. Scale bars: 100 µm. (D) Schematic of the treatment conditions used to generate presomitic mesoderm cells from NOTCHi or DMSO NMPs. (E) Immunofluorescence analysis of the expression of TBXT, SOX2 and TBX6 in DMSO, NOTCHi and NOTCHi-DMSO presomitic mesoderm cultures. Scale bars: 100 µm. (F) Quantification of expression levels of the indicated proteins shown in E based on image analysis of average mean grey value (MGV) per nuclei. Error bars represent mean±s.e.m. (n=3 independent experiments). *P≤0.05, **P≤0.01 (unpaired, two-tailed t-test). (G) qPCR expression analysis of the indicated HOX genes in hESC-derived NOTCHi/control NMPs. Error bars represent mean±s.e.m. (n=3 independent experiments). *P≤0.05, **P≤0.01 (one-sample t-test and Wilcoxon test).

between Notch and HOX gene expression control. Heterochronic grafting experiments have indicated that the global Hox gene expression profile of axial progenitors is plastic as it can be ‘reset’ in response to extrinsic cues emanating from the NMP niche (McGrew et al., 2008). We have also previously shown that hESC-derived NMPs, in which *TBXT* is knocked down via a tetracycline (Tet)-inducible, short hairpin RNA (shRNA)-mediated system (Bertero et al., 2016) (TiKD) are marked by reduced Notch activity as well as an inability to induce properly HOX PG(1-9) members (Gogolou et al., 2022). Given that Notch signalling is typically encoded via receptor–ligand interaction between neighbouring cells, we tested whether it could influence/rescue HOX gene expression in a non-cell-autonomous manner. To this end, we mixed TiKD hESCs with isogenic wild-type hESCs constitutively expressing a red fluorescent protein reporter (H9-RFP), at a 50:50 ratio. The co-cultures were differentiated toward NMPs and treated with Tet to mediate *TBXT* knockdown specifically in the unlabelled TiKD fraction, in the presence or absence of DAPT (Fig. 2A). Following

Development (2024) 151, dev202098. doi:10.1242/dev.202098

NMP differentiation, TBXT knockdown/RFP-negative cells were sorted by fluorescence-activated cell sorting (FACS) from the co-cultures and the levels of HOX transcripts were assayed by qPCR and compared with +Tet and −Tet NMPs derived from TiKD hESCs without co-culture (Fig. 2A, Fig. S3A,B). We found that Tet-induced *TBXT* knockdown was efficient in TiKD cells cultured either alone or together with their wild-type counterparts (Fig. 2B). Tet-induced TBXT knockdown triggered a significant decrease in the expression of most HOX genes and the Notch target *HES5* (Fig. 2B,C, Fig. S3C, compare black versus light blue bars), as previously reported (Gogolou et al., 2022). Strikingly, this trend was partially reversed in TiKD cells upon co-culture with H9-RFP cells: the expression of some HOX genes, particularly those belonging to the *HOXB* PG(5-9), was restored back to levels similar to the −Tet controls (Fig. 2C, Fig. S3C compare black versus light blue versus purple bars). Moreover, upon co-culture with H9-RFPs, TiKD cells exhibited a large increase in the levels of *HES5* (above the −Tet control levels, possibly owing to the reduced levels of the Notch signalling antagonist *DLL3* in TiKD cells; Gogolou et al., 2022; Ladi et al., 2005), suggesting that Notch overactivation takes place specifically under these conditions (Fig. 2B, compare black versus light blue versus purple bars). As expected, this was counteracted by DAPT treatment (Fig. 2B, compare purple versus pink bars), which simultaneously appeared to prevent, mainly in *HOXB* cluster members, the gene expression compensatory effect of the co-culture on TiKD NMPs (Fig. 2C, Fig. S3C compare purple versus pink bars). Co-culture/DAPT treatment did not alter the expression of *TBXT* relative to the Tet-treated TiKD cells cultured alone (Fig. 2B, compare black versus light blue versus purple versus pink bars). Collectively, these results suggest that Notch signalling can control the expression of at least a fraction of the HOX genes expressed by NMPs in a non-cell-autonomous and TBXT-independent manner.

Notch amplifies FGF activity in NMPs

To understand further how Notch signalling influences NMP specification/HOX gene expression, we assessed its crosstalk with the two key posteriorising signalling pathways driving embryonic axis elongation: Wnt and FGF. Thus, we generated NMPs from hESCs in the presence of either DAPT or DMSO as described above (Figs 1A, 3A) and assessed the expression of Wnt/FGF signalling pathway components by qPCR. The transcript levels of Wnt target genes, such as *AXIN2*, *LEF1* and *TCF1* (*TCF7*), remained unchanged

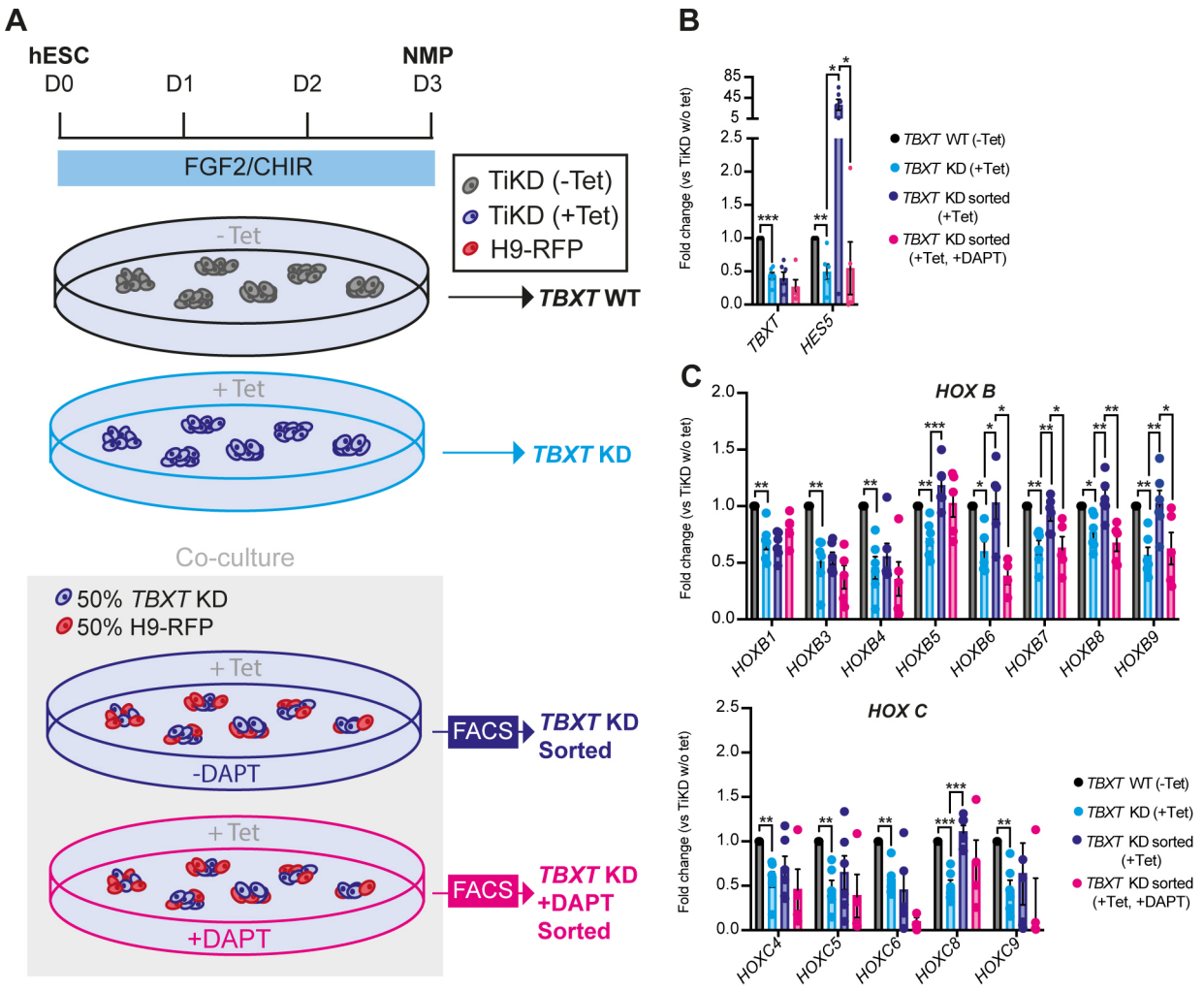

Fig. 2. Notch signalling-dependent rescue of HOX gene expression in TBXT-depleted NMPs. (A) Scheme depicting the experimental design of the *TBXT* shRNA-wild-type NMP co-culture experiment. (B,C) qPCR expression analysis of *TBXT* and *HES5* (B) and HOX genes belonging to paralogous groups B and C (C) under the different experimental conditions depicted in A. Error bars represent mean±s.e.m (n=3-6 independent experiments). *$P\leq0.05$, **$P\leq0.01$, ***$P\leq0.001$ {one-sample t-test and Wilcoxon test [TiKD without Tet versus TiKD (+Tet)] or an unpaired, two-tailed t-test [TiKD (+Tet) versus TiKD sorted (+Tet) versus TiKD (+DAPT +Tet)]}. KD, knockdown; WT, wild type.

Development (2024) 151, dev202098. doi:10.1242/dev.202098

in NOTCHi conditions, whereas expression of *SPRY4*, an FGF signalling target gene, was diminished (Fig. 3B), indicating that Notch inhibition results in a reduction of FGF signalling activity. To confirm this, we examined the levels of the phosphorylated FGF effector kinase ERK1/2 (MAPK) by western blot (Fig. 3C). Both phosphorylated p44 and p42 versions were reduced in NOTCHi NMPs compared with the DMSO-treated controls (Fig. 3C,D), further supporting the notion that Notch positively regulates FGF signalling in hESC derived NMPs. We further tested this by examining whether the NOTCHi NMP phenotype can be rescued by boosting FGF signalling levels via an increase in FGF2 levels. We found that doubling the dosage of FGF2 from 20 to 40 ng/ml, in the presence of DAPT, during NMP induction from hESCs led to an increase in the expression of TBXT and all HOX genes examined, back to levels comparable to those in the DMSO controls (Fig. 3E-G), although it did not rescue TBX6 expression. Conversely, differentiation of hESCs toward NMPs in the absence of FGF2 and presence of the FGF pathway MEK1/2 inhibitor PD0325901 (PD03) and CHIR alone (FGFi) appeared to phenocopy the effects of NOTCHi: *TBX6* expression was significantly reduced whereas the transcript levels of the pro-neural marker *SOX2* increased (Fig. 3H); we have previously shown a reduction in TBXT expression under these conditions (Gogolou et al., 2022). Unlike

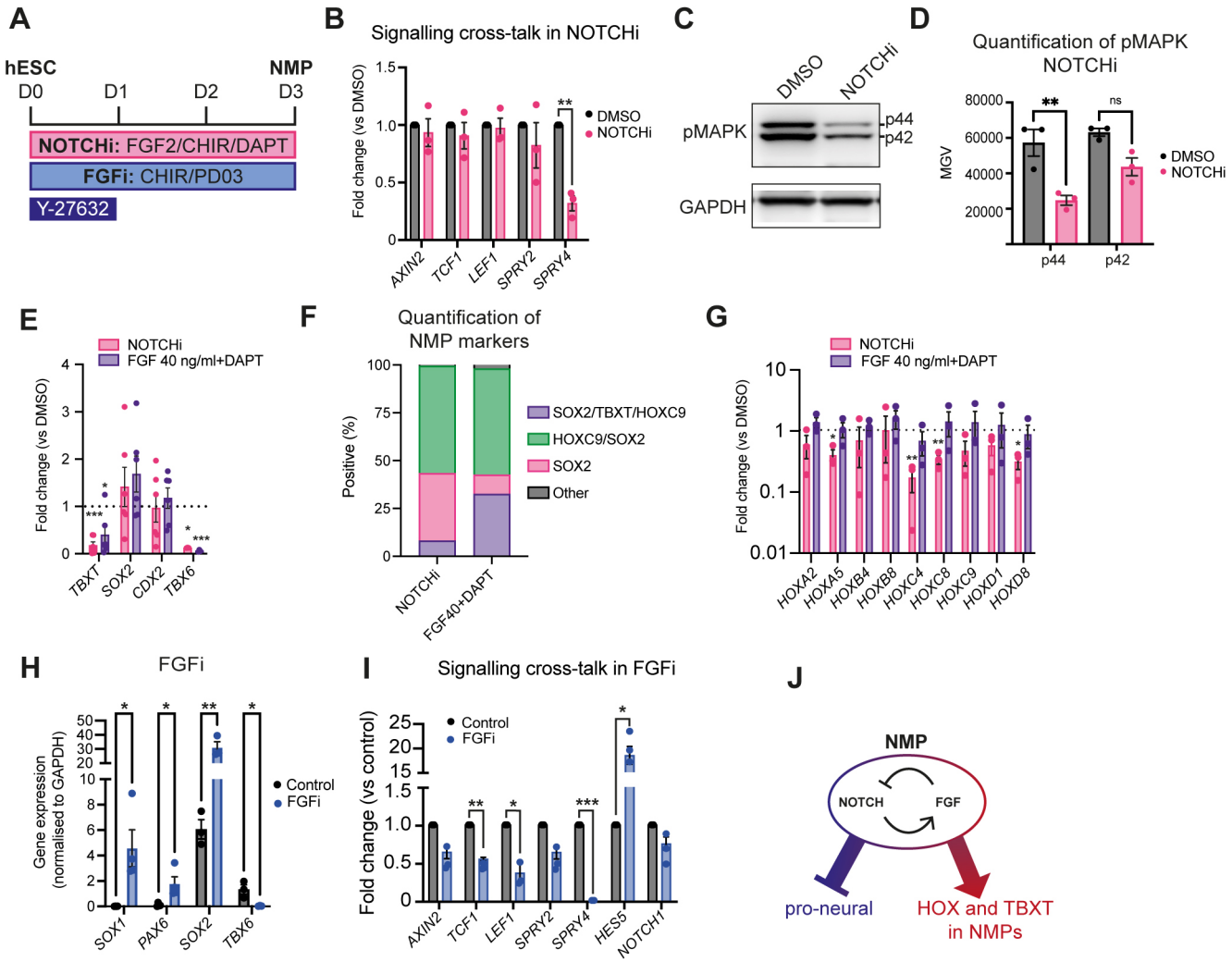

Fig. 3. Notch-FGF signalling crosstalk in hESC-derived NMPs. (A) Scheme of treatments during the differentiation of hESCs toward NMPs. (B) qPCR expression analysis of the indicated Wnt, FGF and Notch signalling pathway components in DAPT/DMSO-treated hESC-derived NMP cultures. Error bars represent mean±s.e.m. (*n*=3 independent experiments). ***P*≤0.01 (one-sample *t*-test and Wilcoxon test). (C,D) Representative western blot analysis of phospho-MAPK (p42/p44) in NOTCHi/DMSO-treated NMPs (C) and corresponding quantification (D). Error bars represent mean±s.e.m. (*n*=3 independent experiments). ***P*≤0.01 (paired two-tailed *t*-test). MGV, mean grey value; ns, not significant. (E) qPCR expression analysis of NMP markers in NOTCHi NMPs generated from hESCs using the standard (20 ng/ml) or high (40 ng/ml) FGF2 concentration. Error bars represent mean±s.e.m. (*n*=6 independent experiments). **P*≤0.05, ****P*≤0.001 (one-sample *t*-test and Wilcoxon test). (F) Image analysis of the percentage of nuclei positive for TBXT, HOXC9 and SOX2 protein expression. Graph shows mean values (*n*=3 independent experiments). NOTCHi data are taken from Fig. S2B. (G) qPCR expression analysis of the indicated HOX genes in NOTCHi NMPs generated from hESCs using the standard (20 ng/ml) or high (40 ng/ml) FGF2 concentration. Error bars represent mean±s.e.m. (*n*=3 independent experiments) **P*≤0.05, ***P*≤0.01 (one-sample *t*-test and Wilcoxon test). (H) qPCR expression analysis of indicated pro-neural/mesodermal NMP and spinal cord neurectoderm markers in PD03-treated (FGFi) hESC-derived NMPs versus controls. Error bars represent mean±s.e.m. (*n*=3 independent experiments). **P*≤0.05, ***P*≤0.01 (paired, two-tailed *t*-test). (I) qPCR expression analysis of indicated Wnt, FGF and Notch signalling pathway components in PD03-treated/control hESC-derived NMP cultures. Error bars represent mean±s.e.m. (*n*=3 independent experiments). **P*≤0.05, ***P*≤0.01 ****P*≤0.001 (one-sample *t*-test and Wilcoxon test). (J) Model depicting the crosstalk between Notch and FGF signalling in regulating HOX/proneural gene and TBXT expression in TBXT^{+}/SOX2^{+} NMPs.

Development (2024) 151, dev202098. doi:10.1242/dev.202098

NOTCHi, the definitive neuroectoderm genes PAX6 and SOX1 were found to be significantly upregulated in FGFi conditions (Fig. 3H). Expression of the FGF targets *SPRY2* and *SPRY4* was robustly reduced, confirming efficient FGF signalling inhibition under these conditions (Fig. 3I). FGF inhibition also resulted in a reduction of Wnt signalling components, in line with findings from analysis of the embryonic NMP niches (Oginuma et al., 2017; Olivera-Martinez et al., 2012). Collectively, our data, combined with our previous observations showing that CHIR-PD03-treated hESC-derived NMPs are marked by global reduction of HOX gene expression as well as *TBXT* (Gogolou et al., 2022), strongly suggest that Notch signalling contributes to the induction of these genes via its, direct or indirect, crosstalk with FGF signalling. Interestingly, FGF inhibition also led to a dramatic increase in the levels of the Notch target *HES5* (Fig. 3I), consistent with previous findings showing that ERK1/2 acts as a negative regulator of γ-secretase, potentially mediating a feedback loop between Notch and FGF signalling (Jaroonwitchawan et al., 2016; Kim et al., 2006) (Fig. 3J).

Notch controls axial progenitor cell fate decisions *in vivo*

We next examined the role of Notch signalling in NMP differentiation *in vivo*. To this end, wild-type and transgenic chicken embryos ubiquitously expressing green fluorescent protein (GFP) were incubated until Hamburger Hamilton (HH) (Hamburger and Hamilton, 1951) stage 4 and then dissected from the egg and cultured *in vitro* until HH8, i.e. the time window that coincides with the emergence of NMPs in the posterior growth region (Guillot et al., 2021) (Fig. 4A). Embryos were cultured on media plates containing either the γ-secretase Notch inhibitor LY411575 (LY) (Wong et al., 2004) or DMSO (control). Following *in vitro* culture,

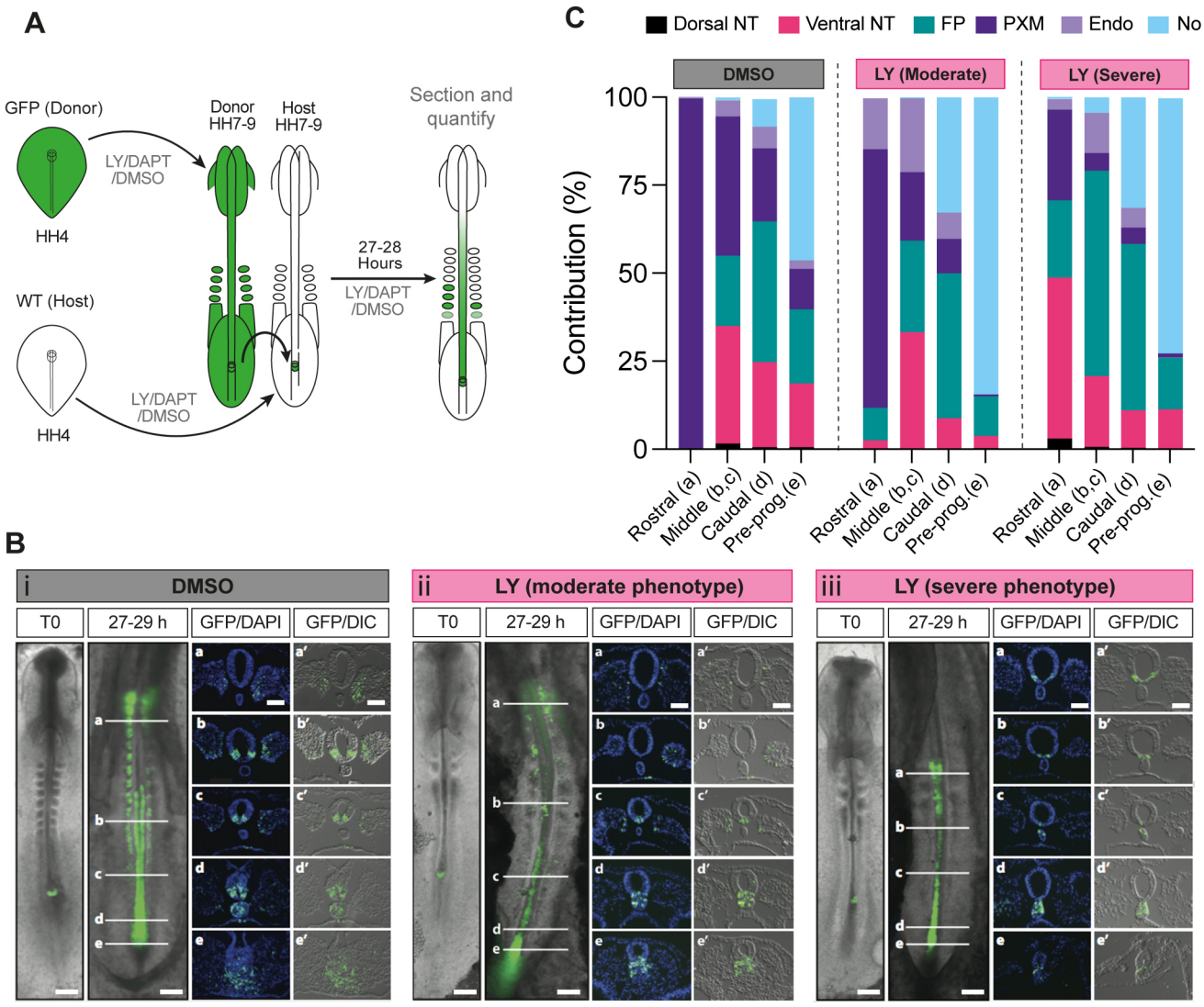

Fig. 4. Notch signalling influences the contribution profile of axial progenitor cells *in vivo*. (A) Scheme depicting the experimental design/treatment regimens of chick embryo grafting experiments. WT, wild type. (B) Whole-mount embryo at the time of receiving an NSB graft (T0) and the GFP contribution pattern following culture in the presence of DMSO (i) or the Notch inhibitor LY in both the moderate (ii) and severe (iii) phenotype embryos after 27-29 h following the graft. Scale bars: 500 µm. Transverse sections at the level of the white indicator lines (a, b, c, d, e) show the nuclear stain DAPI and GFP or DIC with GFP (a′, b′, c′, d′, e′). Images are representative of independent experiments (analysed sectioned embryos: DMSO *n*=9, LY severe *n*=4/9 and moderate *n*=5/9). (C) Quantification of the proportion of GFP cells in transverse sections at position a (rostral), b and c (middle), d (caudal) and e (pre-progenitor, pre-prog.) contributing to axial and paraxial structures [dorsal neural tube (dorsal NT), ventral neural tube (ventral NT), floor plate (FP), paraxial mesoderm (somites rostrally and presomitic mesoderm caudally, PXM), endoderm (Endo) and the notochord (No)] in DMSO and LY-treated cultures.

Development (2024) 151, dev202098. doi:10.1242/dev.202098

the NSB region from DMSO- or LY-treated HH8 GFP transgenic donor chicks was isolated and grafted to a homotopic location on stage-matched DMSO- or LY-treated wild-type host embryos, respectively (Fig. 4A). The host embryos were returned to their respective *in vitro* culture plates (LY or DMSO) and allowed to develop for a further 27-29 h to allow for progenitor cells within the NSB to contribute to axial and paraxial tissues (Fig. 4B). The contribution of GFP^+ donor cells along the axis was then scored according to their final anteroposterior location and subdivided into four domains: rostral, middle, caudal and pre-progenitor (see a-e in Fig. 4B).

Fluorescence microscopy analysis of grafted host embryos revealed that in both DMSO (n=9) and LY treatment (n=9) conditions the extent of donor cell contribution along the anteroposterior axis was similar (Fig. S4A). We found that, in the case of DMSO-treated embryos, GFP-labelled donor axial progenitors contributed almost exclusively to paraxial mesoderm (>99%) in the rostral domain whereas in the more posterior domains (middle, caudal and pre-progenitor), GFP^+ cells were detected in both paraxial mesoderm and the ventral/floor plate segments of the neural tube (Fig. 4B,C, Fig. S4B) reflecting the neuromesodermal bipotency of the grafted donor NSB fragments. The contribution of the donor cells to the dorsal neural tube in the middle, caudal and pre-progenitor domains was minimal whereas the number of donor cells in the notochord increased in an anterior-posterior direction (Fig. 4B,C; n= 9). These findings are in line with previous studies demonstrating the presence of ventral neural tube/floor plate/notochord-biased axial progenitors located in the early somite-stage NSB/node in amniote embryos (Cambray and Wilson, 2007; Catala et al., 1996; Mugele et al., 2018; Selleck and Stern, 1991; Wilson and Beddington, 1996; Wymeersch et al., 2016). We also detected a few GFP^+ cells in the gut within the caudal/pre-progenitor (anterior streak) domains, likely reflecting the inclusion of early node or anterior primitive streak-located endoderm progenitors (Fig. 4B,C, Fig. S4B) (Selleck and Stern, 1991; Wilson and Beddington, 1996). In contrast, the most severely affected LY-treated embryos (‘severe’; n=4/9) exhibited very little/no PXM contribution of GFP^+ donor cells in the rostral and middle domains, where their presence was mainly confined to the floor plate and the ventral neural tube. In the caudal/pre-progenitor domains, LY-treated cells increasingly committed to a notochord fate (Fig. 4B,C, Fig. S4B). A second class of LY-associated ‘moderate’ (n=5/9) phenotype embryos displaying intermediate features between the DMSO and severe LY treatments was also identified (Fig. 4B,C, Fig. S4B). A similar loss of PXM contribution in the rostral/middle regions was also observed in DAPT-treated embryos (n=4) (Fig. S4A-D). Collectively, these findings suggest that Notch signalling preferentially biases NSB-located NMPs to contribute to the paraxial mesodermal lineage at the expense of a ventral neural tube/floor plate fate.

In summary, here we demonstrate that Notch is a central component of the signalling environment within the NMP niche. We show that Notch signalling influences early specification/differentiation of NMPs by steering them toward a presomitic/paraxial mesoderm fate at the expense of neurectoderm. *In vitro*, this appears to be mediated via a negative-feedback loop between Notch and FGF signalling that is possibly required for the proper calibration of the balanced production of neural and mesodermal cells from NMPs. Functional interactions between the two pathways have also been reported during the transition of axial progenitor-derived pre-neural and presomitic mesoderm cells toward spinal cord neurectoderm and somitic mesoderm, respectively (Akai et al., 2005; Anderson et al., 2020; Diaz-Cuadros et al., 2020). Interestingly, these studies indicate that impaired FGF signalling leads to a loss of Notch activity/attenuation of Notch target gene oscillations, suggesting that the relationship between these two pathways is cell type/developmental context specific. Moreover, Notch signalling activity in the NSB/node embryonic regions at earlier stages of development was found to regulate progenitor cell contribution to the floor plate at the expense of notochord (Gray and Dale, 2010). Finally, we show that Notch signalling is also crucial for HOX gene activation in nascent NMPs during their induction from pluripotent cells, a cardinal hallmark of early posteriorisation of embryonic cells. This finding extends previous work linking control of *Hoxd* transcription and Notch signalling (Zákány et al., 2001). Our data suggest that Notch possibly exerts this role in NMPs through regulation of FGF signalling, a well-established driver of HOX gene transcription in the posterior growth region/axial progenitors (Delfino-Machín et al., 2005; Gogolou et al., 2022; Hackland et al., 2019; Mouilleau et al., 2021; van Rooijen et al., 2012). Notch-mediated control of expression of some HOX genes also appears to take place in a non-cell-autonomous manner, as indicated by their DAPT-sensitive transcriptional rescue in Notch-deficient/*TBXT*-depleted hESC-derived NMPs upon co-culture with their wild-type counterparts. The role of the extrinsic environment in influencing cellular Hox codes has been pointed out previously with the demonstration that chick tail bud NMPs can switch from a Hox PG10+ to an ‘earlier’ Hox PG8+ identity following transplantation into the NSB of younger host embryos (McGrew et al., 2008). We propose that Notch signalling is an integral part of the signalling environment within the NMP niche and a crucial regulator of posterior body patterning.

MATERIALS AND METHODS

Cell culture and differentiation

Use of hESCs has been approved by the Human Embryonic Stem Cell UK Steering Committee (SCSC15-23). The following hESC lines were employed: WA09 (H9), H9-RFP and *TBXT* shRNA sOPTiKD hESC lines (H9 background) (Bertero et al., 2016; Thomson et al., 1998). All cell lines were cultured routinely in feeder-free conditions in either Essential 8 (A1517001, Thermo Fisher Scientific, or made in-house) or mTeSR1 (85850, Stem Cell Technologies) medium on Geltrex LDEV-Free reduced growth factor basement membrane matrix (A1413202, Thermo Fisher Scientific). Cells were passaged twice a week after reaching approximately 80% confluency using PBS/EDTA or ReLeSR™ (100-0484, Stem Cell Technologies) as a dissociation reagent. *TBXT* inducible knockdown in the *TBXT* shRNA sOPTiKD hESC line was achieved using tetracycline hydrochloride (Tet) (87128, Merck Life Science) at 1 µg/ml as described previously (Bertero et al., 2016; Gogolou et al., 2022). hESCs were cultured in the presence/absence of Tet for 2 days prior to the initiation of differentiation and the Tet treatment was continued throughout the differentiation for the periods indicated in the Results section and in figures. The RFP hESC line was generated following introduction of a pCAG-H2B-RFP plasmid (Price et al., 2021) into H9 hESCs using a 4D-Nucleofector (Lonza). After puromycin selection (1 µg/ml), single-cell deposition onto feeder cells was carried out followed by culture in 50% mTESR1:50% KnockOut™ Serum Replacement (10829018, Thermo Fisher Scientific) media, 20 µM cholesterol (C1231, Synthechol, Sigma-Aldrich), 10 µM ROCK inhibitor (A11001, Adooq Biosciences). The resulting clones were expanded, manually picked and cultured subsequently in mTeSR1. All cells were screened for *Mycoplasma* using the Lookout Mycoplasma PCR detection kit (MP0040A, Sigma-Aldrich) or Mycostrip *Mycoplasma* detection kit (rep-mys-50, InvivoGen). All cells were routinely screened for indicators of pluripotency: OCT4, NANOG (Table S1) and SSEA4 (Adewumi et al., 2007; Draper et al., 2002).

For NMP differentiation, hESCs (70-80% confluent) were dissociated using Accutase solution (A6964, Merck Life Science) or TrypLE Select (12563029, Gibco) and plated at a density of 60,000 cells/cm^2 on vitronectin (VTN-N) (A31804, Thermo Fisher Scientific)-coated culture plates in

Development (2024) 151, dev202098. doi:10.1242/dev.202098

N2B27 basal medium containing 50:50 Dulbecco's Modified Eagle's Medium (DMEM) F12 (D6421, Merck Life Science)/Neurobasal medium (21103049, Gibco) and 1×N2 supplement (17502001, Gibco), 1×B27 (17504001, Gibco), 1×GlutaMAX (35050061, Gibco), 1×Minimum Essential Medium Non-Essential Amino Acids (MEM NEAA) (11140050, Gibco), 2-mercaptoethanol (50 µM, 31350010, Gibco). The N2B27 medium was supplemented with CHIR (3 µM, 4423, Tocris) and FGF2 (20 ng/ml, 233-FB-500/CF, R&D Systems). The Rho-associated coil kinase (ROCK) inhibitor Y-27632 2HCl (10 µM, A11001, Adooq Biosciences) was added for the first day of NMP induction, as previously described, to aid survival following plating as a single-cell suspension (Frith et al., 2018; Gouti et al., 2017). For late NMP induction, cells were plated at 45,000 cells/cm^2 in N2B27 medium supplemented with CHIR (3 µM) and FGF2 (20 ng/ml) and cultures were fed with fresh supplemented media for 3 days. Y-27632 2HCl (10 µM) was added for the first day only. For presomitic mesoderm induction, cells were plated at 45,000 cells/cm^2 in N2B27 medium supplemented with CHIR (8 µM) and FGF2 (40 ng/ml) and cultures were fed with fresh supplemented media for 3 days. Y-27632 2HCl (10 µM) was added for the first day only. DAPT (2634, Tocris) was added at a concentration of 50 µM and DMSO (D2650, Sigma-Aldrich) was used at 5 µl/ml as control. PD032590 (PZ0162-5MG, Merck) was used at 1 µM. For *TBXT* inducible knockdown, NMP medium was supplemented with 1 µg/ml Tet and replenished every other day.

Analysis of published scRNA-seq data

k-NN plots of induced pluripotent stem cell-derived presomitic mesoderm were generated using an online, interactive, single-cell sequencing tool: https://kleintools.hms.harvard.edu/tools/springViewer_1_6_dev.html?datasets/Diaz2019/hIPSC/full (Diaz-Cuadros et al., 2020).

Flow cytometry

After co-culture of 50% unlabelled TiKD and 50% RFP$^+$ wild-type hESCs and differentiation towards NMP, unlabelled NMPs were sorted at day 3 of differentiation using a FACSJazz cell sorter (BD Biosciences). Gates were set using unlabelled and RFP$^+$ cells independently. Purity checks were carried out post-sorting. Data were analysed with FlowJo software (BD) (See Fig. S2).

Immunofluorescence and imaging

Cells were fixed in 4% paraformaldehyde (J61899.AP, VWR) for 10 min at room temperature, rinsed twice with PBS and permeabilised/blocked with blocking buffer [0.1% Triton X-100 (X100-500 ML, Sigma-Aldrich) and 1% bovine serum albumin (A7906-100G, Sigma-Aldrich)] for 1-2 h at room temperature (RT). Primary antibodies were diluted in the blocking buffer and cells were incubated with primary antibodies overnight at 4°C. Following three washes with PBS, cells were incubated with secondary antibodies conjugated to Alexa fluorophores (Invitrogen) diluted in blocking buffer for 2-4 h at RT, in the dark. Cell nuclei were counterstained with DAPI in PBS (62248, Thermo Fisher Scientific, 1:12000) and fluorescent images were acquired using the InCell Analyser 2200 system (GE Healthcare). Images then were processed in Fiji (Schindelin et al., 2012) or CellProfiler (Stirling et al., 2021) using identical brightness/contrast settings to allow comparison between different treatments. The positive/negative threshold (75th percentile) was set using a sample incubated with secondary antibody only. Antibodies and corresponding dilutions are given in Table S1.

Western blotting

Pelleted cells lysed in RIPA lysis buffer [50 mM Tris-HCl pH8.0, 100 mM NaCl, 2 mM $MgCl_2$, 1% Triton X-100, 0.1% sodium deoxycholate, 0.1% SDS supplemented with 1 mM DTT, 1× Complete protease inhibitor cocktail (11697498001, Roche) and 250 U benzonase nuclease immediately before use] for 10 mins at 37°C followed by centrifugation at 17,000 ***g*** for 2 min to remove insoluble debris, then 50 µg of protein lysate per lane was run on a NuPage 4-12% Bis-Tris gel (NP0322BOX, Thermo Fisher Scientific) at 120 V. Proteins were then transferred to a nitrocellulose membrane (Trans-Blot Turbo Mini 0.2 µm Nitrocellulose Transfer) using Trans-Blot Turbo Transfer System (1704158, Bio-Rad) following the manufacturer's guidelines. Membranes were then washed in TBS-T [Tris-buffered saline with 0.1% Tween 20 detergent (Thermo Fisher Scientific)] and blocked in 5% bovine serum albumin in TBS-T for 1 h at RT. Membrane was incubated with primary antibodies (Table S1) overnight at 4°C followed by horseradish peroxidase-conjugated secondary antibodies for 1 h at RT. ECL detection was enhanced using SuperSignal West Pico PLUS (34580, Thermo Fisher Scientific) as per the manufacturer's guidelines and imaged using a G:BOX Chemi XX98 imager (Syngene). Images then were processed in Fiji (Schindelin et al., 2012).

Quantitative real-time PCR

Total RNA was extracted using the total RNA purification kit (17200, Norgen Biotek) following the manufacturer's instructions. The cDNA synthesis was completed using the High-Capacity cDNA Reverse Transcription kit (4368814, Thermo Fisher Scientific). Quantitative real-time PCR was carried out using the QuantStudio 12 K Flex (Applied Biosystems) thermocycler in combination with the Roche UPL system and the TaqMan Fast Universal PCR Master Mix (4366073, Applied Biosystems) or with PowerUp SYBR Master Mix (A25780, Thermo Fisher Scientific). Primer sequences and corresponding probes (where applicable) are shown in Table S2. Graphs were generated using GraphPad Prism (GraphPad Software), which was also employed for statistical analysis.

Chick embryo grafting experiments

White Leghorn *Gallus* (eggs obtained from Henry Stewart & Co., Lincolnshire and Winter Farm, Royston, UK) or GFP-expressing chick embryos (Roslin Institute, Midlothian, UK; McGrew et al., 2004) were incubated until HH4 and then dissected from the egg and cultured *in vitro* until HH8. Embryos were cultured on media plates containing either a γ-secretase inhibitor dissolved in the solvent DMSO or on media plates containing DMSO alone. The concentration of the γ-secretase inhibitor LY411575 (made in-house, University of Dundee, UK) used was 150 nM. Embryos were transferred to fresh culture plates every 12 h to maintain optimal inhibitor activity. Following *in vitro* culturing, the NSB region from HH8 GFP transgenic donor chicks was isolated and grafted to a homotopic location on stage-matched, wild-type donor embryos. Embryos were then returned to *in vitro* culture plates for a further 27-29 h to allow for progenitor cells within the NSB to contribute to axial and paraxial tissues. Subsequently, embryos were fixed, cryosectioned and analysed by cell count for tissues that were colonised by GFP-positive cells across the rostral, middle, caudal and pre-progenitor domains. Each embryo had five sections from each axial domain analysed by cell count analysis in each domain. The proportion of counted cells in a particular tissue from one section was scored as a proportion of the total GFP-positive cells in that section. The proportion of cells in a particular section was used for analysis as opposed to the raw values obtained in order to avoid variation in cell number between sections and embryos from biasing the analysis. The proportion data on GFP-positive cells in axial and paraxial tissues were pooled between embryos of the same treatment group and axial domain to obtain a mean value. These values therefore represent the mean proportion of cell contribution to specific tissues at specific anterior-posterior axial locations. Pairwise comparisons were made between the GFP cell counts of LY- and DMSO-treated embryos in each cell type at each of the rostral, middle, caudal and pre-progenitor domains and were subjected to an uncorrected Fishers LSD *t*-test to determine where significant differences occurred.

Acknowledgements

We thank Prof. Ivana Barbaric (University of Sheffield) for providing the H2B-RFP expression vector. We are grateful to Matt French, Sally Lowell, Matt Towers, Val Wilson and Sarah Bray for feedback/critical reading of the manuscript.

Competing interests

The authors declare no competing or financial interests.

Author contributions

Conceptualization: F.C., J.K.D., A.T.; Formal analysis: F.C., C.S., S.H., S.G.; Investigation: F.C., C.S., S.H., S.G., K.B., A.G., T.J.R.F., D.S., B.M.J.; Resources:

A.G., T.J.R.F., D.S.; Writing - original draft: F.C., A.T.; Writing - review & editing: F.C., C.S., S.H., S.G., K.B., A.G., T.J.R.F., D.S., B.M.J., D.B., J.K.D.; Visualization: C.S., S.H., S.G., J.K.D.; Supervision: A.T.; Project administration: A.T.; Funding acquisition: D.B., J.K.D., A.T.

Funding

This work was supported by funding from the Biotechnology and Biological Sciences Research Council (BBSRC) (BB/P000444/1), the European Union Horizon 2020 Framework Programme (H2020-EU.1.2.2; grant agreement ID 824070) and the Medical Research Council (MRC) (MR/V002163/1) (to A.T.). K.B. was supported by a White Rose BBSRC Doctoral Training Partnership (DTP) in Mechanistic Biology studentship (BB/T007222/1). S.G. was supported by an MRC New Investigator award to J.K.D. (G0400349: 'Analysis of primitive streak stem cells and the role of Notch in their axial mesoderm derivatives'). Open Access funding provided by the Medical Research Council. Deposited in PMC for immediate release.

Data availability

All relevant data can be found within the article and its supplementary information.

The people behind the papers

This article has an associated 'The people behind the papers' interview with some of the authors.

Peer review history

The peer review history is available online at https://journals.biologists.com/dev/lookup/doi/10.1242/dev.202098.reviewer-comments.pdf

References

Adewumi, O., Aflatoonian, B., Ahrlund-Richter, L., Amit, M., Andrews, P. W., Beighton, G., Bello, P. A., Benvenisty, N., Berry, L. S., Bevan, S. et al. (2007). Characterization of human embryonic stem cell lines by the international stem cell initiative. *Nat. Biotechnol.* **25**, 803-816. doi:10.1038/nbt1318

Akai, J., Halley, P. A. and Storey, K. G. (2005). FGF-dependent Notch signaling maintains the spinal cord stem zone. *Genes Dev.* **19**, 2877-2887. doi:10.1101/gad.357705

Amin, S., Neijts, R., Simmini, S., van Rooijen, C., Tan, S. C., Kester, L., van Oudenaarden, A., Creyghton, M. P. and Deschamps, J. (2016). Cdx and T Brachyury co-activate growth signaling in the embryonic axial progenitor niche. *Cell Rep.* **17**, 3165-3177. doi:10.1016/j.celrep.2016.11.069

Anand, G. M., Megale, H. C., Murphy, S. H., Weis, T., Lin, Z., He, Y., Wang, X., Liu, J. and Ramanathan, S. (2023). Controlling organoid symmetry breaking uncovers an excitable system underlying human axial elongation. *Cell* **186**, 497-512.e23. doi:10.1016/j.cell.2022.12.043

Anderson, M. J., Magidson, V., Kageyama, R. and Lewandoski, M. (2020). Fgf4 maintains Hes7 levels critical for normal somite segmentation clock function. *eLife* **9**, e55608. doi:10.7554/eLife.55608

Bertero, A., Pawlowski, M., Ortmann, D., Snijders, K., Yiangou, L., Cardoso de Brito, M., Brown, S., Bernard, W. G., Cooper, J. D., Giacomelli, E. et al. (2016). Optimized inducible shRNA and CRISPR/Cas9 platforms for in vitro studies of human development using hPSCs. *Development* **143**, 4405-4418. doi:10.1242/dev.138081

Bettenhausen, B., Hrabe de Angelis, M., Simon, D., Guenet, J. L. and Gossler, A. (1995). Transient and restricted expression during mouse embryogenesis of Dll1, a murine gene closely related to Drosophila Delta. *Development* **121**, 2407-2418. doi:10.1242/dev.121.8.2407

Blassberg, R., Patel, H., Watson, T., Gouti, M., Metzis, V., Delás, M. J. and Briscoe, J. (2022). Sox2 levels regulate the chromatin occupancy of WNT mediators in epiblast progenitors responsible for vertebrate body formation. *Nat. Cell Biol.* **24**, 633-644. doi:10.1038/s41556-022-00910-2

Brown, J. M. and Storey, K. G. (2000). A region of the vertebrate neural plate in which neighbouring cells can adopt neural or epidermal fates. *Curr. Biol.* **10**, 869-872. doi:10.1016/s0960-9822(00)00601-1

Cambray, N. and Wilson, V. (2002). Axial progenitors with extensive potency are localised to the mouse chordoneural hinge. *Development* **129**, 4855-4866. doi:10.1242/dev.129.20.4855

Cambray, N. and Wilson, V. (2007). Two distinct sources for a population of maturing axial progenitors. *Development* **134**, 2829-2840. doi:10.1242/dev.02877

Carrieri, F. A. and Dale, J. K. (2016). Turn it down a Notch. *Front. Cell Dev. Biol.* **4**, 151. doi:10.3389/fcell.2016.00151

Catala, M., Teillet, M.-A., Robertis, E. M. D. and Douarin, N. M. L. (1996). A spinal cord fate map in the avian embryo: while regressing, Hensen's node lays down the notochord and floor plate thus joining the spinal cord lateral walls. *Development* **122**, 2599-2610. doi:10.1242/dev.122.9.2599

Chal, J., Oginuma, M., Al Tanoury, Z., Gobert, B., Sumara, O., Hick, A., Bousson, F., Zidouni, Y., Mursch, C., Moncuquet, P. et al. (2015). Differentiation of pluripotent stem cells to muscle fiber to model Duchenne muscular dystrophy. *Nat. Biotechnol.* **33**, 962-969. doi:10.1038/nbt.3297

Chawengsaksophak, K., de Graaff, W., Rossant, J., Deschamps, J. and Beck, F. (2004). Cdx2 is essential for axial elongation in mouse development. *Proc. Natl. Acad. Sci. USA* **101**, 7641-7645. doi:doi:10.1073/pnas.0401654101

Cooper, F., Gentsch, G. E., Mitter, R., Bouissou, C., Healy, L. E., Rodriguez, A. H., Smith, J. C. and Bernardo, A. S. (2022). Rostrocaudal patterning and neural crest differentiation of human pre-neural spinal cord progenitors in vitro. *Stem Cell Rep.* **17**, 894-910. doi:10.1016/j.stemcr.2022.02.018

Dale, J. K., Maroto, M., Dequeant, M. L., Malapert, P., McGrew, M. and Pourquie, O. (2003). Periodic notch inhibition by lunatic fringe underlies the chick segmentation clock. *Nature* **421**, 275-278. doi:10.1038/nature01244

de la Pompa, J. L., Wakeham, A., Correia, K. M., Samper, E., Brown, S., Aguilera, R. J., Nakano, T., Honjo, T., Mak, T. W., Rossant, J. et al. (1997). Conservation of the Notch signalling pathway in mammalian neurogenesis. *Development* **124**, 1139-1148. doi:10.1242/dev.124.6.1139

Delfino-Machín, M., Lunn, J. S., Breitkreuz, D. N., Akai, J. and Storey, K. G. (2005). Specification and maintenance of the spinal cord stem zone. *Development* **132**, 4273-4283. doi:10.1242/dev.02009

Deschamps, J. and Duboule, D. (2017). Embryonic timing, axial stem cells, chromatin dynamics, and the Hox clock. *Genes Dev.* **31**, 1406-1416. doi:10.1101/gad.303123.117

Diaz-Cuadros, M., Wagner, D. E., Budjan, C., Hubaud, A., Tarazona, O. A., Donelly, S., Michaut, A., Al Tanoury, Z., Yoshioka-Kobayashi, K., Niino, Y. et al. (2020). In vitro characterization of the human segmentation clock. *Nature* **580**, 113-118. doi:10.1038/s41586-019-1885-9

Diez del Corral, R., Breitkreuz, D. N. and Storey, K. G. (2002). Onset of neuronal differentiation is regulated by paraxial mesoderm and requires attenuation of FGF signalling. *Development* **129**, 1681-1691. doi:10.1242/dev.129.7.1681

Donoviel, D. B., Hadjantonakis, A. K., Ikeda, M., Zheng, H., Hyslop, P. S. and Bernstein, A. (1999). Mice lacking both presenilin genes exhibit early embryonic patterning defects. *Genes Dev.* **13**, 2801-2810. doi:10.1101/gad.13.21.2801

Draper, J. S., Pigott, C., Thomson, J. A. and Andrews, P. W. (2002). Surface antigens of human embryonic stem cells: changes upon differentiation in culture. *J. Anat.* **200**, 249-258. doi:10.1046/j.1469-7580.2002.00030.x

Dunwoodie, S. L., Henrique, D., Harrison, S. M. and Beddington, R. S. (1997). Mouse Dll3: a novel divergent Delta gene which may complement the function of other Delta homologues during early pattern formation in the mouse embryo. *Development* **124**, 3065-3076. doi:10.1242/dev.124.16.3065

Frith, T. J. R., Granata, I., Wind, M., Stout, E., Thompson, O., Neumann, K., Stavish, D., Heath, P. R., Ortmann, D., Hackland, J. O. S. et al. (2018). Human axial progenitors generate trunk neural crest cells in vitro. *eLife* **7**, e35786. doi:10.7554/eLife.35786

Galceran, J., Sustmann, C., Hsu, S. C., Folberth, S. and Grosschedl, R. (2004). LEF1-mediated regulation of Delta-like1 links Wnt and Notch signaling in somitogenesis. *Genes Dev.* **18**, 2718-2723. doi:10.1101/gad.1249504

Gibb, S., Zagorska, A., Melton, K., Tenin, G., Vacca, I., Trainor, P., Maroto, M. and Dale, J. K. (2009). Interfering with Wnt signalling alters the periodicity of the segmentation clock. *Dev. Biol.* **330**, 21-31. doi:10.1016/j.ydbio.2009.02.035

Gogolou, A., Souilhol, C., Granata, I., Wymeersch, F. J., Manipur, I., Wind, M., Frith, T. J. R., Guarini, M., Bertero, A., Bock, C. et al. (2022). Early anteroposterior regionalisation of human neural crest is shaped by a pro-mesodermal factor. *eLife* **11**, 374263. doi:10.7554/eLife.74263

Gouti, M., Delile, J., Stamataki, D., Wymeersch, F. J., Huang, Y., Kleinjung, J., Wilson, V. and Briscoe, J. (2017). A gene regulatory network balances neural and mesoderm specification during vertebrate trunk development. *Dev. Cell* **41**, 243-261.e7. doi:10.1016/j.devcel.2017.04.002

Gray, S. D. and Dale, J. K. (2010). Notch signalling regulates the contribution of progenitor cells from the chick Hensen's node to the floor plate and notochord. *Development* **137**, 561-568. doi:10.1242/dev.041608

Guibentif, C., Griffiths, J. A., Imaz-Rosshandler, I., Ghazanfar, S., Nichols, J., Wilson, V., Göttgens, B. and Marioni, J. C. (2021). Diverse routes toward early somites in the mouse embryo. *Dev. Cell* **56**, 141-153.e6. doi:10.1016/j.devcel.2020.11.013

Guillot, C., Djeffal, Y., Michaut, A., Rabe, B. and Pourquié, O. (2021). Dynamics of primitive streak regression controls the fate of neuromesodermal progenitors in the chicken embryo. *eLife* **10**, e64819. doi:10.7554/eLife.64819

Hackland, J. O. S., Frith, T. J. R. and Andrews, P. W. (2019). Fully defined and xeno-free induction of hPSCs into neural crest using top-down inhibition of BMP signaling. *Methods Mol. Biol.* **1976**, 49-54. doi:10.1007/978-1-4939-9412-0_4

Hamburger, V. and Hamilton, H. L. (1951). A series of normal stages in the development of the chick embryo. *J. Morphol.* **88**, 49-92. doi:doi:10.1002/jmor.1050880104

Jaroonwitchawan, T., Muangchan, P. and Noisa, P. (2016). Inhibition of FGF signaling accelerates neural crest cell differentiation of human pluripotent stem cells. *Biochem. Biophys. Res. Commun.* **481**, 176-181. doi:doi:10.1016/j.bbrc.2016.10.147

Javali, A., Misra, A., Leonavicius, K., Acharyya, D., Vyas, B. and Sambasivan, R. (2017). Co-expression of Tbx6 and Sox2 identifies a novel transient

neuromesoderm progenitor cell state. *Development* **144**, 4522-4529. doi:10.1242/dev.153262

Kim, S. K., Park, H. J., Hong, H. S., Baik, E. J., Jung, M. W. and Mook-Jung, I. (2006). ERK1/2 is an endogenous negative regulator of the gamma-secretase activity. *FASEB J.* **20**, 157-159. doi:10.1096/fj.05-4055fje

Koch, F., Scholze, M., Wittler, L., Schifferl, D., Sudheer, S., Grote, P., Timmermann, B., Macura, K. and Herrmann, B. G. (2017). Antagonistic activities of Sox2 and brachyury control the fate choice of neuro-mesodermal progenitors. *Dev. Cell* **42**, 514-526.e7. doi:10.1016/j.devcel.2017.07.021

Ladi, E., Nichols, J. T., Ge, W., Miyamoto, A., Yao, C., Yang, L. T., Boulter, J., Sun, Y. E., Kintner, C. and Weinmaster, G. (2005). The divergent DSL ligand Dll3 does not activate Notch signaling but cell autonomously attenuates signaling induced by other DSL ligands. *J. Cell Biol.* **170**, 983-992. doi:10.1083/jcb.200503113

Lippmann, E. S., Williams, C. E., Ruhl, D. A., Estevez-Silva, M. C., Chapman, E. R., Coon, J. J. and Ashton, R. S. (2015). Deterministic HOX patterning in human pluripotent stem cell-derived neuroectoderm. *Stem Cell Rep.* **4**, 632-644. doi:10.1016/j.stemcr.2015.02.018

Martin, B. L. and Kimelman, D. (2012). Canonical Wnt signaling dynamically controls multiple stem cell fate decisions during vertebrate body formation. *Dev. Cell* **22**, 223-232. doi:10.1016/j.devcel.2011.11.001

McGrew, M. J., Sherman, A., Ellard, F. M., Lillico, S. G., Gilhooley, H. J., Kingsman, A. J., Mitrophanous, K. A. and Sang, H. (2004). Efficient production of germline transgenic chickens using lentiviral vectors. *EMBO Rep.* **5**, 728-733. doi:10.1038/sj.embor.7400171

McGrew, M. J., Sherman, A., Lillico, S. G., Ellard, F. M., Radcliffe, P. A., Gilhooley, H. J., Mitrophanous, K. A., Cambray, N., Wilson, V. and Sang, H. (2008). Localised axial progenitor cell populations in the avian tail bud are not committed to a posterior Hox identity. *Development* **135**, 2289-2299. doi:10.1242/dev.022020

Metzis, V., Steinhauser, S., Pakanavicius, E., Gouti, M., Stamataki, D., Ivanovitch, K., Watson, T., Rayon, T., Mousavy Gharavy, S. N., Lovell-Badge, R. et al. (2018). Nervous system regionalization entails axial allocation before neural differentiation. *Cell* **175**, 1105-1118.e17. doi:10.1016/j.cell.2018.09.040

Mouilleau, V., Vaslin, C., Robert, R., Gribaudo, S., Nicolas, N., Jarrige, M., Terray, A., Lesueur, L., Mathis, M. W., Croft, G. et al. (2021). Dynamic extrinsic pacing of the HOX clock in human axial progenitors controls motor neuron subtype specification. *Development* **148**, dev194514. doi:10.1242/dev.194514

Mugele, H., Plummer, A., Baritello, O., Towe, M., Brecht, P. and Mayer, F. (2018). Accuracy of training recommendations based on a treadmill multistage incremental exercise test. *PLoS One* **13**, e0204696. doi:10.1371/journal.pone.0204696

Mukherjee, S., Luedeke, D. M., McCoy, L., Iwafuchi, M. and Zorn, A. M. (2022). SOX transcription factors direct TCF-independent WNT/β-catenin responsive transcription to govern cell fate in human pluripotent stem cells. *Cell Rep.* **40**, 111247. doi:doi:10.1016/j.celrep.2022.111247

Nakaya, M. A., Biris, K., Tsukiyama, T., Jaime, S., Rawls, J. A. and Yamaguchi, T. P. (2005). Wnt3a links left-right determination with segmentation and anteroposterior axis elongation. *Development* **132**, 5425-5436. doi:10.1242/dev.02149

Neijts, R., Amin, S., van Rooijen, C., Tan, S., Creyghton, M. P., de Laat, W. and Deschamps, J. (2016). Polarized regulatory landscape and Wnt responsiveness underlie Hox activation in embryos. *Genes Dev.* **30**, 1937-1942. doi:10.1101/gad.285767.116

Neijts, R., Amin, S., van Rooijen, C. and Deschamps, J. (2017). Cdx is crucial for the timing mechanism driving colinear Hox activation and defines a trunk segment in the Hox cluster topology. *Dev. Biol.* **422**, 146-154. doi:10.1016/j.ydbio.2016.12.024

Nowotschin, S., Ferrer-Vaquer, A., Concepcion, D., Papaioannou, V. E. and Hadjantonakis, A.-K. (2012). Interaction of Wnt3a, Msgn1 and Tbx6 in neural versus paraxial mesoderm lineage commitment and paraxial mesoderm differentiation in the mouse embryo. *Dev. Biol.* **367**, 1-14. doi:doi:10.1016/j.ydbio.2012.04.012

Oginuma, M., Moncuquet, P., Xiong, F., Karoly, E., Chal, J., Guevorkian, K. and Pourquié, O. (2017). A gradient of glycolytic activity coordinates FGF and Wnt signaling during elongation of the body axis in amniote embryos. *Dev. Cell* **40**, 342-353.e10. doi:10.1016/j.devcel.2017.02.001

Oka, C., Nakano, T., Wakeham, A., de la Pompa, J. L., Mori, C., Sakai, T., Okazaki, S., Kawaichi, M., Shiota, K., Mak, T. W. et al. (1995). Disruption of the mouse RBP-J kappa gene results in early embryonic death. *Development,* **121**, 3291-3301. doi:10.1242/dev.121.10.3291

Olivera-Martinez, I., Harada, H., Halley, P. A. and Storey, K. G. (2012). Loss of FGF-dependent mesoderm identity and rise of endogenous retinoid signalling determine cessation of body axis elongation. *PLoS Biol,* **10**, e1001415. doi:10.1371/journal.pbio.1001415

Price, C. J., Stavish, D., Gokhale, P. J., Stevenson, B. A., Sargeant, S., Lacey, J., Rodriguez, T. A. and Barbaric, I. (2021). Genetically variant human pluripotent stem cells selectively eliminate wild-type counterparts through YAP-mediated cell competition. *Dev. Cell* **56**, 2455-2470.e10. doi:10.1016/j.devcel.2021.07.019

Schindelin, J., Arganda-Carreras, I., Frise, E., Kaynig, V., Longair, M., Pietzsch, T., Preibisch, S., Rueden, C., Saalfeld, S., Schmid, B. et al. (2012). Fiji: an open-source platform for biological-image analysis. *Nat. Methods* **9**, 676-682. doi:10.1038/nmeth.2019

Selleck, M. A. and Stern, C. D. (1991). Fate mapping and cell lineage analysis of Hensen's node in the chick embryo. *Development* **112**, 615-626. doi:10.1242/dev.112.2.615

Semprich, C. I., Davidson, L., Amorim Torres, A., Patel, H., Briscoe, J., Metzis, V. and Storey, K. G. (2022). ERK1/2 signalling dynamics promote neural differentiation by regulating chromatin accessibility and the polycomb repressive complex. *PLOS Biol.* **20**, e3000221. doi:10.1371/journal.pbio.3000221

Shen, W., Huang, J. and Wang, Y. (2021). Biological significance of NOTCH signaling strength. *Front. Cell Dev. Biol.* **9**, 652273. doi:10.3389/fcell.2021.652273

Souilhol, C., Perea-Gomez, A., Camus, A., Beck-Cormier, S., Vandormael-Pournin, S., Escande, M., Collignon, J. and Cohen-Tannoudji, M. (2015). NOTCH activation interferes with cell fate specification in the gastrulating mouse embryo. *Development* **142**, 3649-3660. doi:10.1242/dev.121145

Stirling, D. R., Swain-Bowden, M. J., Lucas, A. M., Carpenter, A. E., Cimini, B. A. and Goodman, A. (2021). CellProfiler 4: improvements in speed, utility and usability. *BMC Bioinformatics* **22**, 433. doi:10.1186/s12859-021-04344-9

Thomson, J. A., Itskovitz-Eldor, J., Shapiro, S. S., Waknitz, M. A., Swiergiel, J. J., Marshall, V. S. and Jones, J. M. (1998). Embryonic stem cell lines derived from human blastocysts. *Science* **282**, 1145-1147. doi:10.1126/science.282.5391.1145

Tsakiridis, A., Huang, Y., Blin, G., Skylaki, S., Wymeersch, F., Osorno, R., Economou, C., Karagianni, E., Zhao, S., Lowell, S. et al. (2014). Distinct Wnt-driven primitive streak-like populations reflect in vivo lineage precursors. *Development* **141**, 1209-1221. doi:10.1242/dev.101014

Turner, D. A., Hayward, P. C., Baillie-Johnson, P., Rué, P., Broome, R., Faunes, F. and Martinez Arias, A. (2014). Wnt/β-catenin and FGF signalling direct the specification and maintenance of a neuromesodermal axial progenitor in ensembles of mouse embryonic stem cells. *Development* **141**, 4243-4253. doi:10.1242/dev.112979

van Rooijen, C., Simmini, S., Bialecka, M., Neijts, R., van de Ven, C., Beck, F. and Deschamps, J. (2012). Evolutionarily conserved requirement of Cdx for post-occipital tissue emergence. *Development* **139**, 2576-2583. doi:10.1242/dev.079848

Verrier, L., Davidson, L., Gierliński, M., Dady, A. and Storey, K. G. (2018). Neural differentiation, selection and transcriptomic profiling of human neuromesodermal progenitor-like cells in vitro. *Development* **145**, dev166215. doi:10.1242/dev.166215

Williams, R., Lendahl, U. and Lardelli, M. (1995). Complementary and combinatorial patterns of Notch gene family expression during early mouse development. *Mech. Dev.* **53**, 357-368. doi:10.1016/0925-4773(95)00451-3

Wilson, V. and Beddington, R. S. (1996). Cell fate and morphogenetic movement in the late mouse primitive streak. *Mech. Dev.* **55**, 79-89. doi:10.1016/0925-4773(95)00493-9

Wind, M., Gogolou, A., Manipur, I., Granata, I., Butler, L., Andrews, P. W., Barbaric, I., Ning, K., Guarracino, M. R., Placzek, M. et al. (2021). Defining the signalling determinants of a posterior ventral spinal cord identity in human neuromesodermal progenitor derivatives. *Development* **148**, dev194415. doi:10.1242/dev.194415

Wong, G. T., Manfra, D., Poulet, F. M., Zhang, Q., Josien, H., Bara, T., Engstrom, L., Pinzon-Ortiz, M., Fine, J. S., Lee, H. J. et al. (2004). Chronic treatment with the gamma-secretase inhibitor LY-411,575 inhibits beta-amyloid peptide production and alters lymphopoiesis and intestinal cell differentiation. *J. Biol. Chem.* **279**, 12876-12882. doi:10.1074/jbc.M311652200

Wymeersch, F. J., Huang, Y., Blin, G., Cambray, N., Wilkie, R., Wong, F. C. K. and Wilson, V. (2016). Position-dependent plasticity of distinct progenitor types in the primitive streak. *eLife* **5**, e10042. doi:10.7554/eLife.10042

Wymeersch, F. J., Skylaki, S., Huang, Y., Watson, J. A., Economou, C., Marek-Johnston, C., Tomlinson, S. R. and Wilson, V. (2019). Transcriptionally dynamic progenitor populations organised around a stable niche drive axial patterning. *Development* **146**, dev168161. doi:10.1242/dev.168161

Wymeersch, F. J., Wilson, V. and Tsakiridis, A. (2021). Understanding axial progenitor biology in vivo and in vitro. *Development* **148**, dev180612. doi:10.1242/dev.180612

Young, T., Rowland, J. E., van de Ven, C., Bialecka, M., Novoa, A., Carapuco, M., van Nes, J., de Graaff, W., Duluc, I., Freund, J. N. et al. (2009). Cdx and Hox genes differentially regulate posterior axial growth in mammalian embryos. *Dev. Cell* **17**, 516-526. doi:10.1016/j.devcel.2009.08.010

Zákány, J., Kmita, M., Alarcon, P., de la Pompa, J.-L. and Duboule, D. (2001). Localized and transient transcription of Hox genes suggests a link between patterning and the segmentation clock. *Cell* **106**, 207-217. doi:10.1016/S0092-8674(01)00436-6

Zhang, N. and Gridley, T. (1998). Defects in somite formation in lunatic fringe-deficient mice. *Nature* **394**, 374-377. doi:10.1038/28625

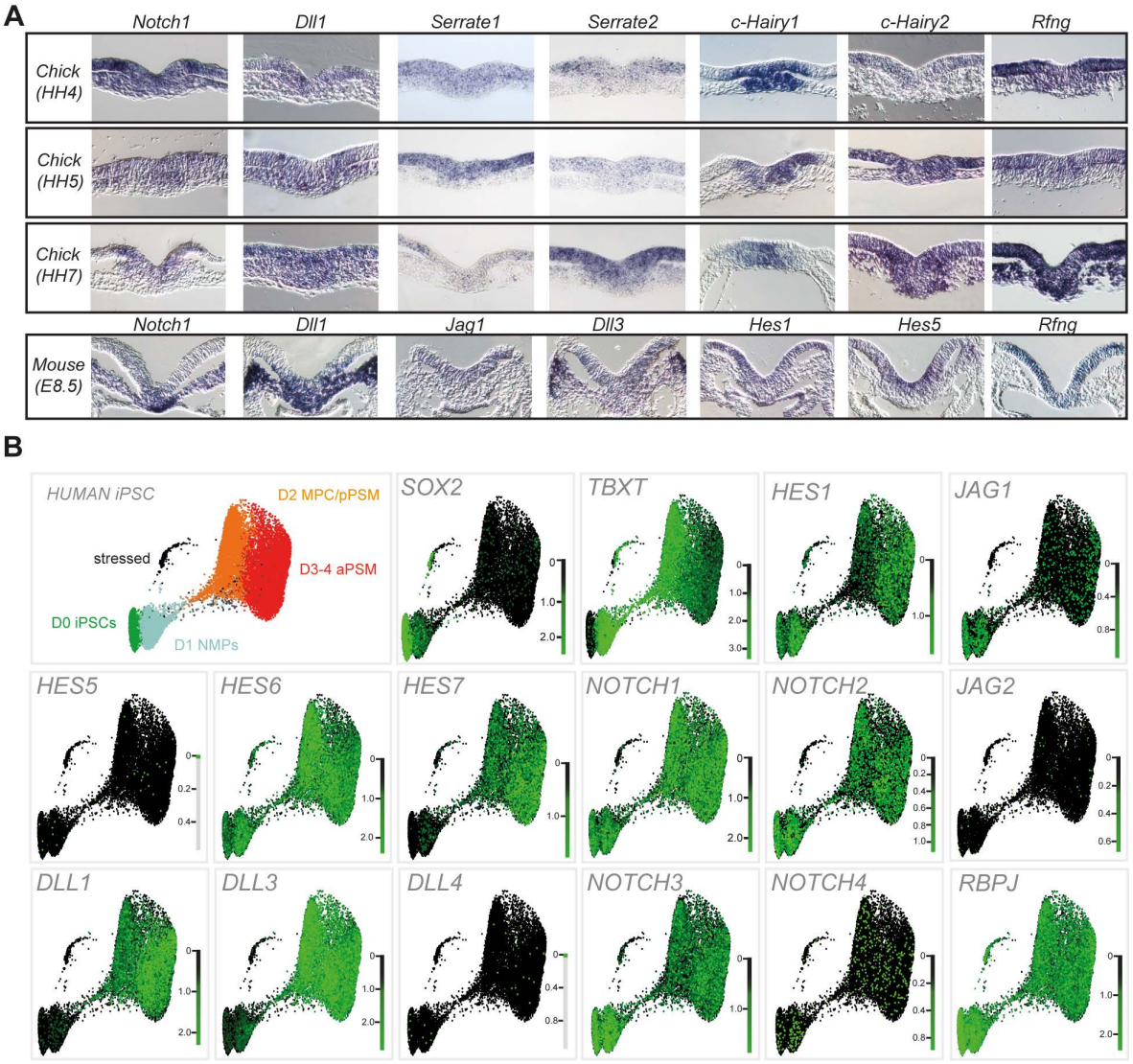

Fig. S1. Expression of Notch signalling components in axial progenitors. (A) *In situ* hybridisation analysis of expression of Notch pathway components in transverse sections of the chick and mouse caudal progenitor area corresponding to the indicated embryonic stages. HH, Hamburger Hamilton, E, embryonic day. (b) ForceAtlas2 layouts of single-cell k-nearest neighbour (kNN) graphs overlaid with log-normalized transcript counts for key components of the Notch pathway in human induced pluripotent stem cells (iPSCs) differentiating toward NMPs and presomitic mesoderm (PSM). Published data obtained from (Diaz-Cuadros et al., 2020). D, differentiation day; aPSM, anterior presomitic mesoderm; pPSM, posterior presomitic mesoderm; MPC, mesodermal precursor cell.

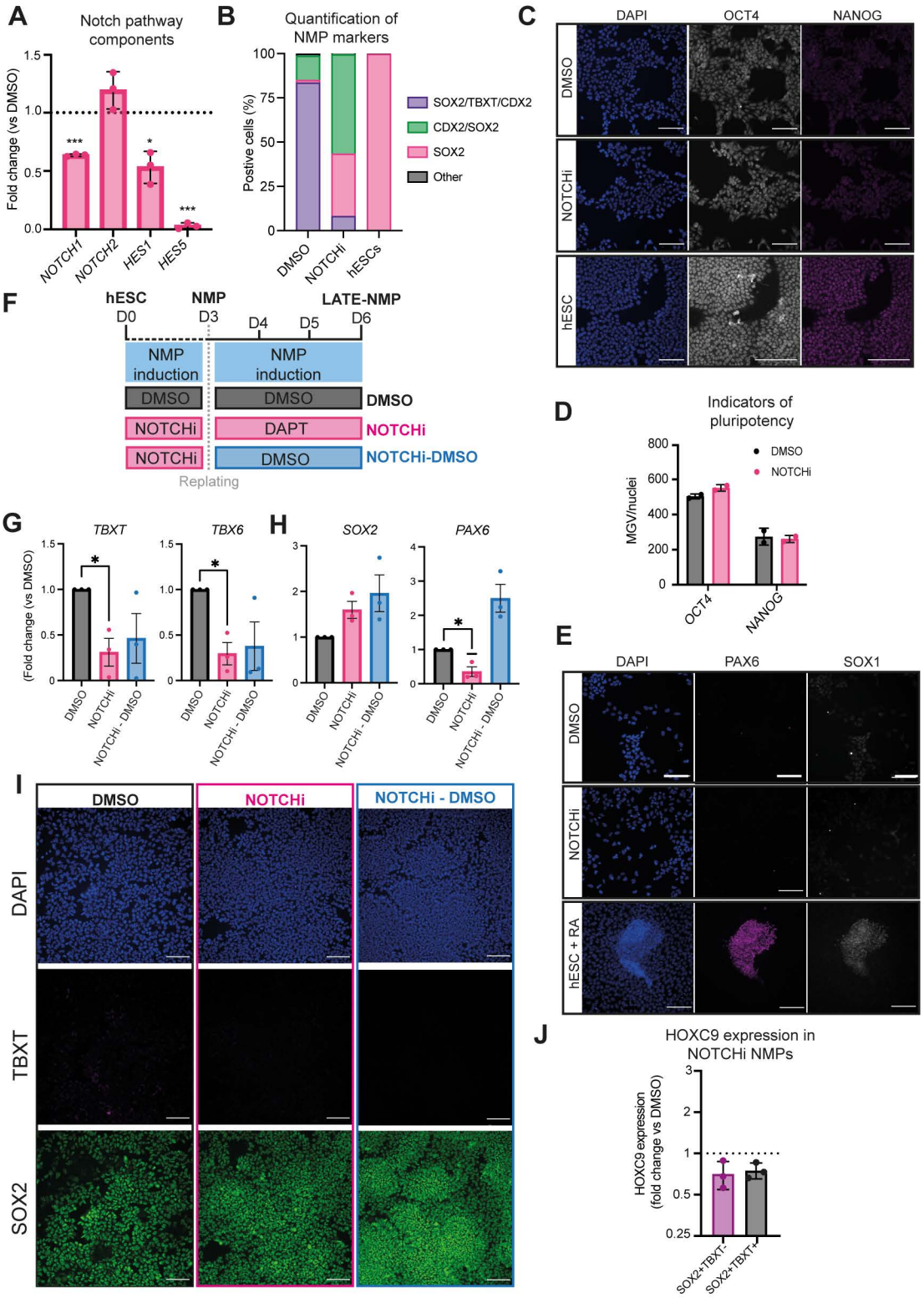

Fig. S2. Effect of Notch signalling inhibition on hESC-derived NMPs. (A) qPCR expression analysis of indicated Notch signalling pathway components/ targets in NOTCHi hESC-derived NMPs compared to DMSO controls. Error bars represent mean±s.e.m n=3. *P≤0.05, **P≤0.01 ***P=≤0.001 (one sample t and Wilcoxon test). (B) Image analysis depicting the percentage of nuclei positive for TBXT, HOXC9 and SOX2 protein expression. Graph shows mean values (n=3

independent experiments) (C) Pluripotency associated marker expression in DMSO and NOTCHi hESC-derived NMPscompared to undifferentiated hESC controls. (D) Quantification of MGV/nuclei for markers shown in (C). Error bars represent mean±s.d. (n=2 independent experiments). (E) Neuroectoderm associated marker expression in DMSO and NOTCHi hESC-derived NMPs compared to a positive control (hESC+RA). RA, retinoic acid (F) Scheme of depicting Notch manipulation conditions during prolonged NMP culture (G,H) qPCR analysis of *TBXT, TBX6, SOX2* and *PAX6* expression in D6 “late NMP” cultures induced using the conditions shown in (F) Error bars represent mean±s.e.m (n=3 independent experiments). *P≤0.05 (I) Immunofluorescence analysis of the expression of TBXT and SOX2 in “late NMP” cultures generated using the indicated conditions. (J) Immunofluorescence analysis of MGV of HOXC9 and SOX2 protein expression relative to TBXT positivity (TBXT+ or TBXT-) in DAPT-treated NMPs. Error bars represent mean±s.e.m (n=3 independent experiments, paired two-tailed t-test).

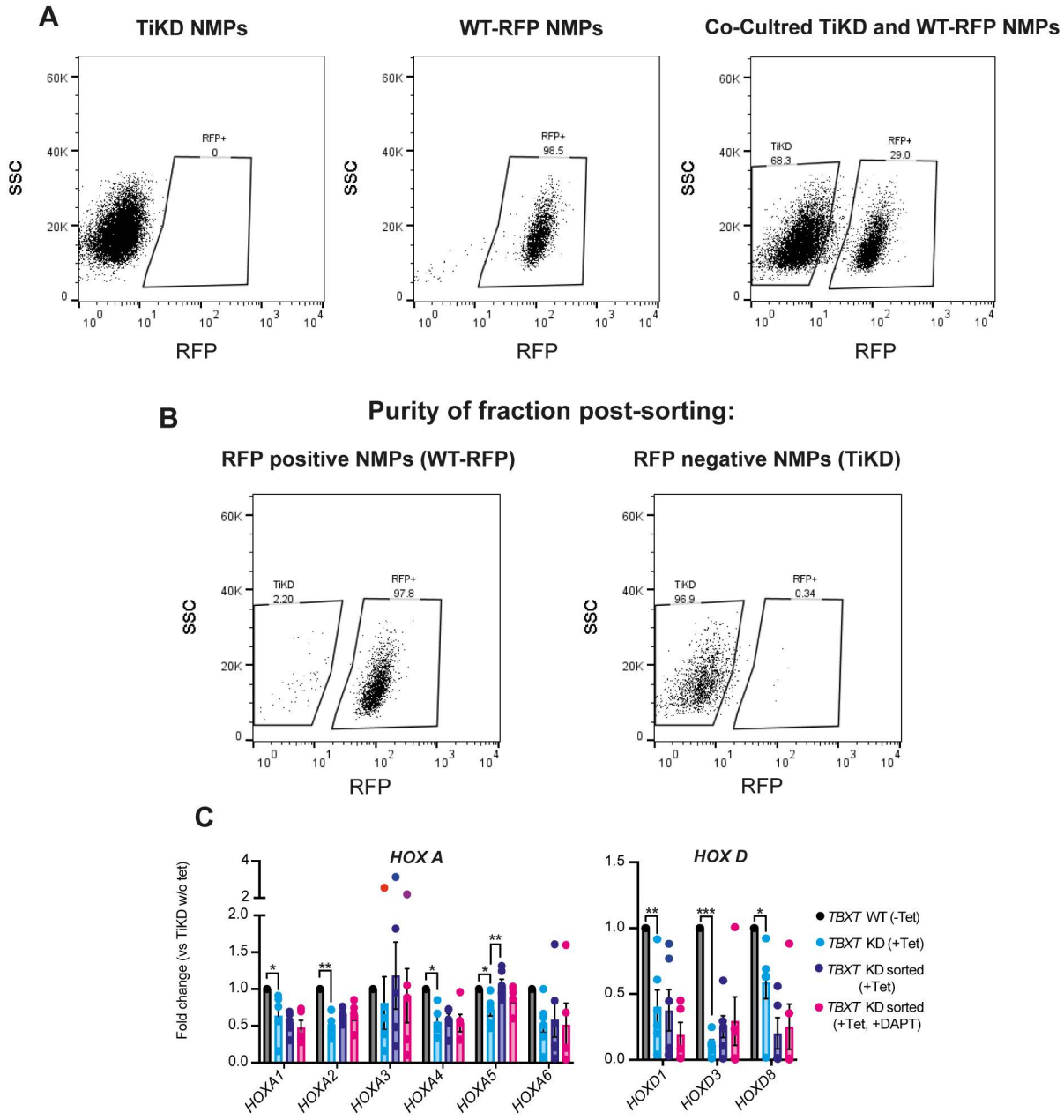

Fig. S3. Manipulation of TBXT expression and Notch signalling activity in co-cultures of hESC-derived NMPs. (A) FACS dot plots showing the fractions of RFP fluorescent reporter-positive cells in unlabelled TBXT knockdown (TiKD), wild type RFP (WT-RFP) hESC-derived NMPs and co-cultured (TiKD and WT-RFP) NMPs. (B) FACS dot plots showing the purity assessment following FACS of co-cultured NMPS into RFP negative (TiKD) and RFP positive (WT-RFP) fractions. (C) qPCR expression analysis of *HOX* genes belonging to paralogous groups A and D under the different experimental conditions depicted in Fig 2A. Error bars represent mean±s.e.m (n=3-6 independent experiments) *P≤0.05, **P≤0.01 ***P=≤0.001 (one sample t and Wilcoxon test (TiKD w/o Tet vs TiKD (+Tet)) or an unpaired two-tailed t.test (TiKD (+Tet) vs TiKD sorted (+tet) vs TiKD (+DAPT +Tet).

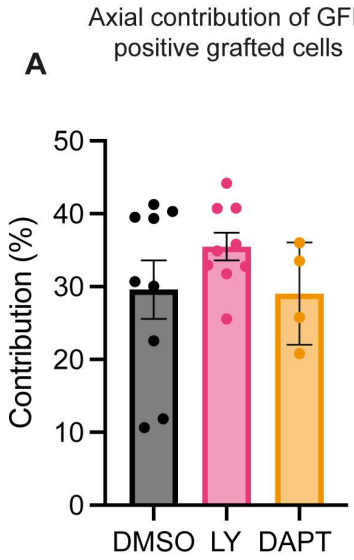

B

Uncorrected Fishers LSD T.Test: Intermediate phenotype

		Dorsal Neural Tube	Ventral Neural Tube	Floor Plate	Paraxial Mesoderm	Endoderm	Notochord
LY vs DMSO	Rostral	ns	ns	ns	ns	*(0.0282)	ns
	Middle	ns	ns	ns	ns	**(0.0054)	ns
	Caudal	ns	ns	ns	ns	ns	**(0.0033)
	Pre-progenitor	ns	ns	ns	ns	ns	**(0.0011)

Uncorrected Fishers LSD T.Test: Severe phenotype

		Dorsal Neural Tube	Ventral Neural Tube	Floor Plate	Paraxial Mesoderm	Endoderm	Notochord
LY vs DMSO	Rostral	ns	***(0.0007)	ns	***(<0.0001)	ns	ns
	Middle	ns	ns	***(0.0003)	**(0.0089)	ns	ns
	Caudal	ns	ns	ns	ns	ns	**(0.0031)
	Pre-progenitor	ns	ns	ns	ns	ns	***(<0.0011)

Uncorrected Fishers LSD T.Test: DAPT

		Dorsal Neural Tube	Ventral Neural Tube	Floor Plate	Paraxial Mesoderm	Endoderm	Notochord
LY vs DMSO	Rostral	***(<0.0001)	***(0.0007)	ns	**(<0.0059)	ns	ns
	Middle	ns	ns	**(0.0056)	ns	ns	ns
	Caudal	ns	ns	ns	ns	ns	ns
	Pre-progenitor	ns	ns	ns	ns	ns	ns

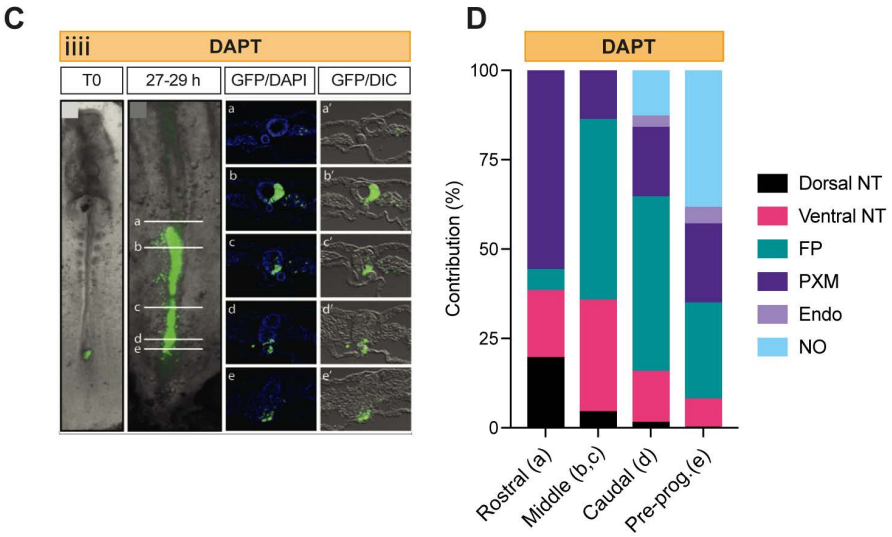

Fig. S4. Axial contribution of chick embryonic axial progenitors in the presence and absence of Notch signalling inhibition. (A) Percentage anterior-posterior embryonic axis colonised by cells from the NSB following DMSO, LY and DAPT treatment. Error bars indicate mean±s.e.m (DMSO n=9, LY n=9, DAPT n=4). ns (unpaired two-tailed t.test). (B) Table showing the statistical P-value results for the severe and moderate LY phenotype using a one-way ANOVA (Fisher's LSD test) (analysed sectioned embryos: DMSO n=9, LY severe n=4/9 and moderate n=5/9 and DAPT n=4). (C) Wholemount embryo at the time of receiving a NSB graft (T0) and the GFP contribution pattern following culture in the presence of the Notch inhibitor DAPT embryos after 27-29 hours following the graft. Transverse sections at the level of the white indicator lines (a, b, c, d, e) show the nuclear show the nuclear stain DAPI and GFP or DIC with GFP (a', b', c', d', e'). Images are representative of independent experiments (analysed sectioned embryos: DAPT = 4. (D) Quantification of the proportion (%) of GFP cells in transverse sections at position a (rostral), b and c (middle), d (caudal) and e (pre-progenitor, pre-prog.) contributing to axial and paraxial structures (dorsal neural tube (dorsal NT), ventral neural tube (ventral NT), floor plate (FP), paraxial mesoderm (somites rostrally and PSM caudally, PXM), endoderm (Endo) and the notochord (No) in DMSO and LY-treated.

Table S1. Antibodies used in this study

Available for download at
https://journals.biologists.com/dev/article-lookup/doi/10.1242/dev.202098#supplementary-data

Table S2. Primer sequences used in this study

Available for download at
https://journals.biologists.com/dev/article-lookup/doi/10.1242/dev.202098#supplementary-data